

FlooNoC: A 645 Gbps/link 0.15 pJ/B/hop Open-Source NoC with Wide Physical Links and End-to-End AXI4 Parallel Multi-Stream Support

Tim Fischer¹, Student Member, IEEE, Michael Rogenmoser¹, Student Member, IEEE, Thomas Benz¹, Student Member, IEEE, Frank K. Gürkaynak¹, and Luca Benini¹, Fellow, IEEE

Abstract—The new generation of domain-specific AI accelerators is characterized by rapidly increasing demands for bulk data transfers, as opposed to small, latency-critical cache line transfers typical of traditional cache-coherent systems. In this paper, we address this critical need by introducing the *FlooNoC* Network-on-Chip (NoC), featuring very wide, fully Advanced eXtensible Interface (AXI4) compliant links designed to meet the massive bandwidth needs at high energy efficiency. At the transport level, non-blocking transactions are supported for latency tolerance. Additionally, a novel end-to-end ordering approach for AXI4, enabled by a multi-stream capable Direct Memory Access (DMA) engine simplifies network interfaces and eliminates inter-stream dependencies.

Furthermore, dedicated physical links are instantiated for short, latency-critical messages. A complete end-to-end reference implementation in 12nm FinFET technology demonstrates the physical feasibility and power performance area (PPA) benefits of our approach. Utilizing wide links on high levels of metal, we achieve a bandwidth of 645 Gbps per link and a total aggregate bandwidth of 103 Tbps for an 8×4 mesh of processors cluster tiles, with a total of 288 RISC-V cores. The NoC imposes a minimal area overhead of only 3.5% per compute tile and achieves a leading-edge energy efficiency of 0.15 pJ/B/hop at 0.8 V. Compared to state-of-the-art NoCs, our system offers three times the energy efficiency and more than double the link bandwidth. Furthermore, compared to a traditional AXI4-based multi-layer interconnect, our NoC achieves a 30% reduction in area, corresponding to a 47% increase in GFLOPS_{DP} within the same floorplan.

Index Terms—Network-On-Chip, AXI, Network Interface, Very large scale integration, Physical Design

I. INTRODUCTION

The demands of modern workloads, particularly Large Language Models (LLMs), have led to the emergence of ultra-large Artificial Intelligence (AI) workload accelerators, fabricated in full reticles of cutting-edge technologies [1]–[3]. These accelerators feature tile-based designs arranged in tiled floorplans and connected with mesh NoCs. Due to the

substantial bandwidth requirements, these systems commonly rely on NoCs designed to support bulk data transfers. Moreover, the memory-intensive nature of these workloads results in massive bandwidth at the boundary of the mesh, as the tiles frequently require expensive off-chip memory accesses [4], [5]. Addressing these issues is crucial, requiring NoCs that are designed for both high bandwidth and latency tolerance to enable asynchronous data processing while maximizing memory bandwidth utilization.

In this paper, we focus on NoCs for the new wave of extreme AI accelerators, optimized for bulk data transfers, typically generated by Direct Memory Access (DMA) engines. Unlike NoCs for cache-coherent systems that are designed to transport cache lines at low latency, bulk-transfer networks are designed to handle large chunks of data efficiently with an emphasis on bandwidth rather than latency. Cache-coherent systems and interconnects, which have also been the subject of intensive investigation, are out-of-scope for this work; we refer the interested reader to existing literature on this topic [6], [7].

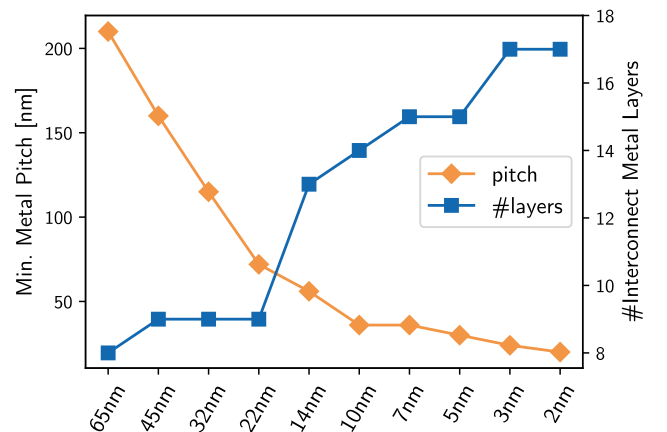


Fig. 1: Technology scaling of on-chip wire resources based on IDRS reports [8] for 2–14 nm and [9] for 22–65 nm.

Delivering large bulks of data to the Processing Elements (PEs) with a sustained high-bandwidth data flow is an unsolved problem at the scale needed today and in the near future. In traditional NoCs, large data transfers are serialized over many flits onto links up to 64 bit in widths [10], with increased

This paper has been submitted to the IEEE for possible publication. Copyright might be transferred without notice, after which this version may no longer be accessible

T. Fischer, M. Rogenmoser, T. Benz, F. K. Gürkaynak, and L. Benini are with the Integrated System Laboratory (IIS), ETH Zurich, Switzerland. E-mail: fischeti, michaero, tbenz, kgf, lbenini@iis.ee.ethz.ch

L. Benini is also with the Department of Electrical, Electronic and Information Engineering (DEI), University of Bologna, Italy.

This work has been supported in part by ‘The European Pilot’ project under grant agreement No 101034126 that receives funding from EuroHPC-JU as part of the EU Horizon 2020 research and innovation programme.

link frequency to satisfy bandwidth requirements. However, this approach encounters significant limitations in modern systems, where bandwidth is ultimately constrained by the on-chip clock frequency, which cannot be raised above a few GHz for power and signal integrity reasons. Consequently, the traditional practice of serialized links requires reassessment in modern NoCs.

Furthermore, as illustrated in Figure 1, recent advancements in on-chip routing resources reveal that within the past decade, the minimum metal pitch in Very Large-Scale Integration (VLSI) technologies has decreased tenfold, while the number of interconnect metal layers has more than doubled. This trend strongly supports a shift towards wider links as opposed to faster links to accommodate the ever-increasing demand for bandwidth.

The trend in technology scaling shown in Figure 1 also calls for a re-evaluation of the use of virtual channels in NoC designs. Traditionally, NoCs have employed virtual channels to enable sharing and the reduction of physical links. However, with the advancements in modern VLSI technologies, which now provide extensive routing resources sufficient for multiple and wide physical links, the justification for using virtual channels is diminishing. Although virtual channels can enhance network routability by reducing the number of wires, they also affect bandwidth efficiency and add complexity to routers due to the need for additional buffering and arbitration between virtual channels. Given these factors, a shift toward physical links over virtual ones is increasingly justified in today's VLSI technologies [11].

Although routing resources in newer technologies are becoming increasingly abundant, merely increasing the width of NoC links is not sufficient for an efficient implementation. Integrating the NoC tightly with logic blocks results in better area utilization compared to their physical separation [12]. However, this integration poses additional challenges, such as potential impacts on compute logic due to the increased routing resource demands of the NoC. Furthermore, NoC designers must consider the physical distances that links must span, adding appropriate buffer cells or elastic buffers to achieve targeted timing [13]. This task is complicated by modern systems incorporating substantial on-chip memory in the form of Static Random-Access Memory (SRAM) macros, which can obstruct buffer placement and block routing on the lower metal layers. Consequently, a deep understanding of the underlying technology and synergy with the physical design flow is essential to navigate these complexities effectively during the NoC design process.

In addition to addressing physical constraints, one must consider how data transfers are managed at the transport level. Non-coherent block data transfers, which require explicit management, typically via DMA engines, provide an efficient way to control data movement on-chip and towards main memory. AXI4, as the prevailing protocol for non-coherent transfers is particularly suited for these tasks. It supports burst transfers and multiple outstanding transactions, enhancing its latency tolerance and making it a preferred choice for non-coherent systems. Despite its advantages and widespread adoption, implementing AXI4 as a network-level protocol in a NoC

introduces significant challenges. Its stringent requirement for transaction ordering based on the Transaction ID (TxnID) complicates operations, as the complexity of monitoring outstanding transactions and maintaining order scales with the network's diameter [14]. This complexity significantly restricts the scalability of multi-hop interconnects that depend on AXI4-compliant links.

Separating the NoC network-level protocol from the AXI4-compliant initiators with Network Interfaces (NIs) [10], [15] addresses the inherent scalability limitations of AXI4 and enables the design of more flexible and scalable interconnect architectures suited for many-core systems. Specifically, implementing a bespoke NoC network-level protocol simplifies the router design significantly. This setup enables packets to be routed based primarily on their destination addresses, while the NIs efficiently handle outstanding transactions and guarantees the ordering of responses. While there has been a surge in open-source NoC implementations [16]–[18], the availability of AXI4-compliant NIs that support multiple transactions and burst transfers remain confined to proprietary industry solutions [19]–[21], whose performance and scalability is not assessed and quantified in the open literature.

A common strategy to implement a high-performance, AXI4-compliant NI that adheres to AXI4's ordering restrictions is to use a Reorder Buffer (RoB) to manage AXI4 responses that arrive out of order from the NoC [22]–[24]. However, this solution presents several significant disadvantages. First, RoBs are costly due to their large memory requirements. For example, with a single AXI4 burst capable of reaching up to 4 kB, the RoB must be sized to accommodate several such bursts to manage multiple outstanding transactions. Second, the performance of the NI is closely tied to the RoB's capacity; transaction processing must be stalled if the RoB is full. Moreover, while RoBs enable the handling of multiple out-of-order transactions, they inherently increase response latency, as each response might be delayed in the buffer before it is forwarded to the AXI4 interface. Consequently, a more holistic end-to-end approach rather than a strictly NI-centric solution, is necessary to address these challenges effectively.

Given all these issues that arise in modern NoCs for high-performance systems, we propose a new NoC design based on the following four principles: **1) Wide links** routed on high metal levels, supporting buffer insertion in the design implementation to mitigate the serialization bottleneck and substantially increasing bandwidth to accommodate data-intensive applications. **2) Physical channels over virtual ones**, enhancing the network's ability to manage diverse traffic types effectively. **3) Full AXI4 support**, enabling multiple outstanding transactions and burst capabilities to meet high-performance requirements efficiently. **4) Decoupling network and transport layers** to solve the scalability issues of AXI4 multi-hop networks.

Compared to our preliminary work [22], we have incorporated several critical improvements to the architecture and present new results. First, we have expanded the NI by introducing a *RoB-less* implementation, significantly enhancing area efficiency. Second, we have integrated a multi-stream capable DMA engine into the compute cluster, which enables

end-to-end ordering more effectively than our previous work. Third, we substantially improved the physical implementation of the NoC, integrating it with a compute cluster into a compute tile, achieving significant advancements across power, performance, and area (PPA) metrics. Furthermore, we have carried out physical implementation on a complete large-scale design comprising 288 RISC-V cores and conducted a detailed PPA analysis for the entire system. Lastly, we carried out a quantitative comparison between *FlooNoC* and an interconnect based on multi-level AXI4-Crossbars (Xbars) design, demonstrating our solution's superior performance and area benefits. The key contributions of this paper are:

- We present (to the best of our knowledge) the first open-source¹ NoC with fully AXI4-compliant initiator and target interfaces that efficiently handle the ordering requirements imposed by AXI4 at the endpoints rather than in the routers while achieving full bandwidth utilization.
- We propose an end-to-end ordering solution that combines a RoB-less implementation of the NI with a multi-stream capable DMA. The tight integration thereof in a compute tile eliminates inter-stream dependencies, offering a streamlined, high-performance solution while reducing area complexity by up to 58%.
- We demonstrate the physical implementation of an 8×4 compute mesh using 12 nm VLSI technology. The NoC integrated into the compute tile accounts for a mere 3.5% of the tile area, yet achieves leading-edge energy-efficiency and performance, delivering 0.15 pJ/B/hop at 0.8 V and an aggregate bandwidth of 103 Tbps at 1.26 GHz in typical conditions, corresponding to a delay of less than 70 Fanout-of-4 Inverter (FO4).
- We present a comprehensive comparison between a System-on-Chip (SoC) designed with traditional AXI4 matrices and our NoC-based solution. Our findings demonstrate that the NoC-based solution achieves a 30% reduction in area for the same core count or delivers 47% higher performance given the same floorplan.

II. BACKGROUND & RELATED WORKS

Research in NoCs has significantly advanced since its inception [15], [25] more than two decades ago, yet many areas remain actively explored. We break down our discussion of related works into three main areas of NoC research tackled by our study. First, we look at efforts to ensure compatibility with the widely-used AXI4 standard and its ordering rules, a critical aspect for interfacing with existing systems. Then, we move on to the development of wide and physical channels essential for high-bandwidth systems. Lastly, we consider the physical awareness of NoC design, stressing the importance of making design choices that align with the physical constraints of VLSI design.

A. Advanced Microcontroller Bus Architecture (AMBA)

The Advanced Microcontroller Bus Architecture (AMBA) is a family of open on-chip protocol specifications developed

by ARM that have continuously evolved to meet the demands of modern systems. AXI4 is a widely-used protocol for high-bandwidth on-chip communication [26] with several well-established open-source implementations [14]. AXI4 defines separate channels for read and write requests (AR, AW, W) and response channels (R, B). It also supports multiple outstanding transactions, which allows memory latency to be hidden at the initiator for a higher system throughput.

The AXI4 protocol enforces strict ordering of transactions using the TxnID, which serves as an identifier for each transaction. The width of the TxnID is determined by the number of initiators and their characteristics. The protocol requires that transactions with the same TxnID are processed in order and, due to its role in routing responses, that the TxnID width increases with each network hop to maintain unique transaction identifiers. This requirement creates challenges in scaling AXI4 for large systems with multiple hops, as it requires managing state information for each TxnID, leading to exponential complexity [14] and limiting scalability. While TxnID remappers [14] can reduce the number of IDs, they introduce significant overhead in latency and area and complicate tracing and verification.

The latest generation of the AMBA family, AMBA5, introduced the Coherent Hub Interface (CHI) protocol, designed for high-performance systems requiring cache coherency. CHI operates at a fine granularity, handling data at the cache line level, and is not optimized for bulk data transfers. In contrast, CHI complements, rather than replaces, AXI4, which is further evidenced by the simultaneous introduction of AXI5, which features performance improvements and enhanced functionality to align with CHI's capabilities. Among them, AXI5 introduced support for Atomic Operations (ATOPs). The main difference between atomic and non-atomic transactions is that the former generates both a read and a write response on the *R*, respectively, *B* channel. To prevent issues related to the ordering of transactions, the AXI4 specification requires that outstanding atomic transactions have a unique TxnID. Furthermore, atomic transactions cannot use the same TxnID as non-atomic transactions that are outstanding.

This work is fully compatible with the AXI4 standard, leveraging its support for multiple outstanding transactions and burst transfer capabilities to achieve high performance. Additionally, we incorporate support for ATOPs, introduced with AXI5, which are essential in manycore systems for data consistency and efficient synchronization of PEs.

B. AXI4 Network-on-Chips

Previous efforts have explored leveraging AXI4 matrices to develop an AXI4-compatible NoC [14], [27], using AXI4-Crosspoints (XPs) in place of traditional routers. Such an AXI4-XP includes a standard AXI4 Xbar equipped with TxnID remappers at each output port, ensuring TxnID width remains constant across the network. However, this method faces several challenges. Each XP incurs substantial logic overhead due to the necessity of tracking outstanding transactions through the crossbar and TxnID remappers. Additionally, maintaining transaction ordering for those with identical IDs

¹<https://github.com/pulp-platform/FlooNoC>

in AXI4-XPs can degrade performance, as it may force new transactions to stall to preserve order.

To address these ordering challenges, RoBs have been suggested to be implemented either at endpoints [23], [24], [28] or within the NoC itself [29]. These solutions include RoB optimizations such as dynamic allocation and tracking entries in "ordering lists" to optimize RoB use and minimize its size [23], [28]. TxnID renaming has also been introduced [24] to manage multiple in-order transactions. Nevertheless, these strategies introduce substantial complexity. They necessitate tables to monitor RoB entries and face limitations due to the potential size of the RoB, which is particularly problematic in high-bandwidth systems. For example, AXI4 supports data widths up to 1024 bit and burst sizes up to 4 kB. Although RoBs may suffice for smaller transactions, they prove to be excessively costly for handling multiple outstanding bursts on the scale of kilobytes.

C. Wide & Physical Channels

In the field of NoC design, especially for systems requiring high bandwidth, recent research [30], as well as commercial-grade chips [31] lean towards employing physical channels over virtual ones. Studies referenced in [32], [33] illustrate that opting for physical channels contributes to both area and power efficiency improvements, which will gain further relevance with the progress in semiconductor technologies, where an abundance of routing resources favors simpler microarchitectures. Routers of physical channel-based NoCs are characterized by reduced buffering requirements and the capability to operate at higher frequencies, thereby boosting overall system performance. Furthermore, the perspective offered in Bill Dally's 2020's NoC symposium keynote [11] underscores the significance of leveraging technological advancements in routing resources, advocating for a shift towards physical channels.

Besides using physical channels over virtual ones, *Ruche* networks [34] have been proposed, introducing additional long-range physical channels that bypass routers in 2D-mesh networks with the goal of decreasing the NoC diameter and bisection bandwidth. They incur a significant cost in terms of area, however, since the router radix increases. Further, in scenarios where traffic is primarily routed towards I/O or memory located at the boundary of a chip, *Ruche* channels will not be able to provide additional bandwidth since traffic will be predominantly routed through *ruce* channels, resulting in lower utilization of the local links.

Splitting a single physical link into multiple subnets rather than using multiple physical links, has been proposed as a strategy to enhance energy efficiency [35]. This approach allows for more fine-grained Power Gating (PG) of the subnets, improving energy management. However, while this method conserves power, it also reduces the bandwidth of the links and introduces latency overheads stemming from additional serialization requirements and the time needed to wake up the subnets.

Wide physical links to achieve higher throughput are common in many commercial products [31], [36] with channel

widths up to 1024 bit. Another study has also reported significant performance gains in Register Transfer Level (RTL) simulation by increasing the link size to 512 bit [37], but its implementation was limited to Field-Programmable Gate Arrays (FPGAs) and actual physical implementation was not demonstrated. There has also been research arguing for smaller flit sizes [7]. However, the authors limited the analysis to virtual channel routers and traffic of coherent general-purpose Central Processing Units (CPUs). Coherent traffic is very different from burst-based non-coherent traffic since it is characterized by a high amount of small control packets. Furthermore, the common assumption the authors use that router area grows quadratically with the channel width has been disputed if physical implementation effects are considered [12].

D. Awareness of Physical Implementation

The physical implementation aspect of NoCs has also been studied in the literature. In [12], the authors analyze the area and wiring resources of NoC routers and conclude that routers are routing-bound and propose *NoC Symbiosis* to absorb the wiring resources of the node logic, which is typically under-utilized. This approach is also evident in industrial solutions with a tile-based design [31], [36], where the NoC is flattened into the tile instead of implemented as a standalone block.

Furthermore, the choice of topology plays a crucial role in the physical design of NoCs. The 2D-mesh, favored for its simplicity and efficiency, is predominantly used in both academic [30], [38]–[41] and commercial implementations [31], [36], [42], [43]. However, exploring tile-based physical design methodologies has not been confined to conventional topologies. More complex arrangements, such as concentrated mesh, *Ruche*, and torus topologies, have been evaluated [44].

A quantitative and comparative PPA analysis of various mesh-based State-of-the-Art (SoA) NoC physical implementations will be presented in Table III. This analysis will explore the trade-offs between achieved bandwidth and the costs in terms of area, as well as the energy efficiency of data transfers, which are crucial considerations in today's High-Performance Computing (HPC) systems.

III. NOC MICROARCHITECTURE

A. Network Interface (NI)

The main task of the NI is to handle the protocol conversion at the endpoint from AXI4 to the network-level protocol while adhering to the ordering requirements of AXI4. AXI4 requires that transactions with the same TxnID are ordered. These ordering guarantees can be satisfied using additional hardware in every switch to track outstanding transactions for each TxnID [14]. However, this results in significant complexity in every hop of the network, drastically limiting scalability. To avoid this complexity, we handle reordering in the NI, allowing us to use simpler NoC routers that do not need to guarantee in-order transactions. The architecture of the NI is shown in Figure 2, which includes an *Ordering Unit*, as shown in orange.

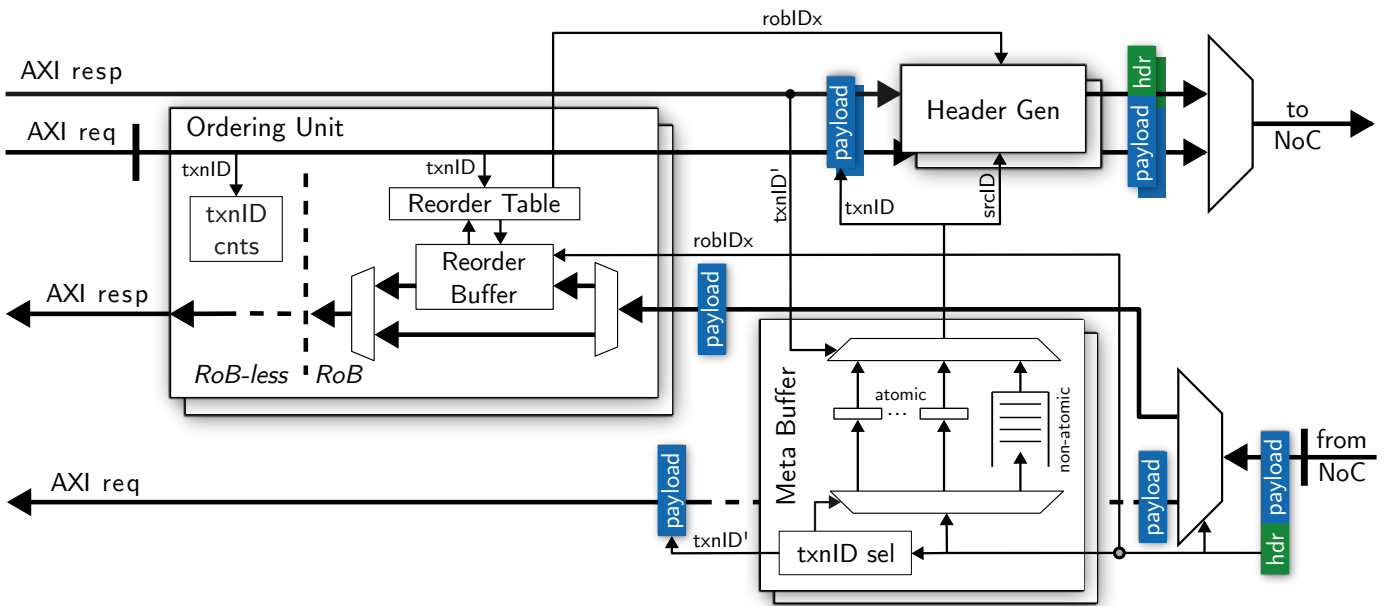


Fig. 2: AXI4 Network Interface architecture for request (AR/AW/W) and response (R/B) paths. Reads and writes are independent in AXI4, and the request/response paths are very similar in the NI and are depicted as overlapping modules. The *Ordering Unit* can be configured with or without reordering capabilities (i.e. *RoB* and *RoB-less*).

The *Ordering Unit* ensures the correct order of AXI4 responses returning to the AXI4 interface. Ordering can be achieved in two different ways: 1) buffering out-of-order responses in a *RoB* and releasing them once they are in order again, and 2) stalling the injection of new requests into the NoC if the responses might arrive out of order, which can happen if two requests target different destinations. Our proposed NI supports both approaches with two different configurations.

1) *Reorder-Capable NI*: The reorder-capable NI, already outlined in [22], features a *RoB* to enable concurrent outstanding transactions to different destinations without violating the ordering of the responses. It does so by keeping track of outstanding transactions in a *Reorder Table* and using end-to-end flow control, meaning new AXI4 requests are only injected into the NoC if there is enough space in the *RoB* to store the response. A response always contains a unique identifier *robIDx*, which is stored in the *Reorder Table* to determine whether it is out of order and needs to be buffered in the *RoB*. Otherwise, the response can be directly forwarded to the AXI4 interface. Apart from being a unique identifier, the *robIDx* also acts as the index into the *RoB*, where it should be stored. The space in the *RoB* is allocated when the request is granted and before injecting into the NoC. This *RoB* allocation happens dynamically, and the generated *robIDx* is pushed into the *Reorder Table*, where it is removed once the response has been forwarded to the AXI4 interface, either from the *RoB* or directly from the NoC. We also implemented two optimizations that reduce the need for *RoB* storage allocation 1) The first response of a stream of transactions with equal TxnID is always in order and does not require allocation 2) Assuming deterministic routing in the network, the responses of requests to the same destination will arrive in the same

order as the requests were issued. Hence, there is no need to reorder them. Those optimizations can be done independently for each TxnID, which allows for the retention of support for out-of-order transactions of different TxnIDs.

2) *RoB-less NI*: We also propose a *RoB-less* NI, a more cost-effective implementation to guarantee the ordering requirements. For each TxnID, a counter tracks the number of outstanding transactions and stalls incoming requests if the *dstID* differs from the previous transactions that are currently outstanding. Assuming a static routing algorithm inside the network, this mechanism already solves the ordering requirements since responses from the same destination are guaranteed to arrive in the same order as the corresponding requests, while responses from different destinations might arrive out of order. The lack of buffering resources makes this solution very cost-effective at the expense of potential performance degradation due to stalls. However, stalls can be prevented if transactions to different destinations are decoupled downstream with different TxnIDs.

3) *Non-Atomic & Atomic Transactions*: On top of AXI4, which only defines non-atomic transactions, we additionally support ATOPs as outlined in [14]. The main difference between ATOPs and non-atomic transactions is that each ATOP has a unique TxnID amongst all outstanding transactions. This requirement has some implications for handling ATOPs in the NI. First, ATOPs can bypass the *Ordering Unit* since it is guaranteed that there are no other outstanding transactions with the same TxnID. Second, ATOPs are treated differently by the *Meta Buffer*, which stores the information required to return the responses to the source (i.e., the *srcID*) in a FIFO. Non-atomic transactions are all mapped to the same TxnID to guarantee ordering downstream, and the *srcID* for the response can be popped from the FIFO in the same order

it was pushed into. ATOPs, however, are allowed to arrive out-of-order. Hence, the *Meta Buffer* has a separate set of buffers to store the return information of ATOPs.

B. Links & Flits

The conventional method of serializing a packet over a narrow link and identifying the start and end with header and tail flits is inefficient for wide physical links. When an entire packet can be transmitted in a single flit on a wide link, the additional header and tail flits reduce the effective bandwidth to 33%. We employ parallel lines for header information, including routing, ordering, and payload type to overcome this limitation as illustrated in Figure 3.

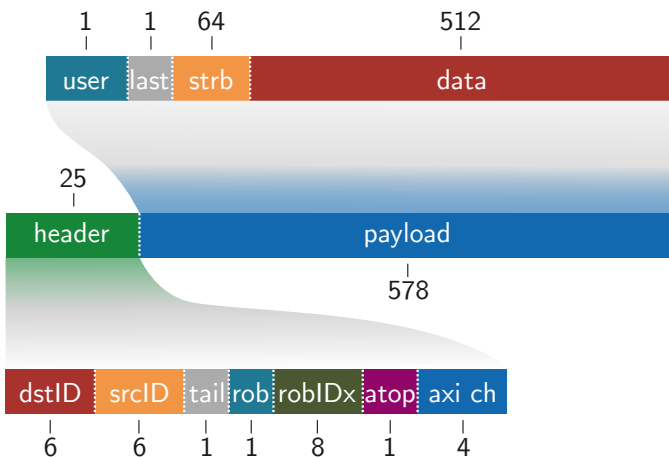


Fig. 3: Example of a single flit, consisting of header information and an AXI W beat payload of 512 bit.

Besides using parallel lines for header information, we also employ separate physical channels to accommodate the diverse traffic requirements within an SoC interconnect. The traffic can vary greatly due to the different types of initiators involved. For instance, programmable DMAs often utilize very wide buses and burst-based data transfers to meet the high bandwidth demands of compute elements. In contrast, compute cores usually generate single-word transfers for tasks such as synchronization and configuration. To cater to these different traffic patterns, we provide dedicated links for latency-sensitive traffic via narrow channels and high-bandwidth traffic via wide channels. The dimensions of both narrow (64-bit) and wide (512-bit) links are configured to fit all packets into a single flit, which can be transmitted in one cycle. This setup enables us to match the frequency and bandwidth of the endpoint AXI4 bus with the NoC links. We implement three physical links in each direction, as Table I details.

AXI4 requests and responses are always transmitted over separate physical links to avoid message-level deadlocks. The *req* and *rsp* links are mainly used for handling latency-sensitive requests and responses from compute cores. In addition, narrow links are utilized for read requests and write responses from the wide AXI4 bus, as these messages do not fully utilize the bandwidth of a wide link. By mapping them to narrow links, the wide link is reserved for high-bandwidth traffic such as read and write bursts.

TABLE I: Description and dimensions of physical links. Mapping of AXI requests and responses of DATAWIDTH = 64/512 bit, ADDRWIDTH = 48 bit.

Phys. link	Size [bits]	Mapping & Primary Payload	
		AXI Narrow	AXI Wide
<i>req</i>	119	AR/AW: 48-bit addr W: 64-bit data	AR: 48-bit addr
<i>rsp</i>	103	R: 64-bit data B: 2-bit resp	B: 2-bit resp
<i>wide</i>	603	-	AW: 48-bit address R/W: 512-bit data

An exception to this approach involves wide write requests, which are mapped to the wide link. Write beats (*W* beats) are not associated with a TxnID, so they must be strictly ordered. This ordering requirement becomes challenging when address write (*AW*) and write data (*W*) are sent over different links and could be interleaved with other write requests from different initiators. To address this issue, write requests and write data are always bundled together, and wormhole routing is used in the NoC to prevent interleaving and maintain order.

C. Router

Our NoC leverages wide physical links and a reduced operating frequency compared to traditional narrow links, offering significant microarchitectural advantages in router design, as illustrated in Figure 4. We utilize simple, low-area, and low-complexity routers that do not require internal pipelining. Furthermore, instead of virtual channels, we implement multilink routers, which include separate routers for each of the three physical links, ensuring complete network isolation. The routers also do not enforce any ordering of flits, which significantly improves scalability compared to interconnects based on AXI4 matrices.

These routers are highly configurable, supporting any number of input and output ports, and use a valid-ready handshake mechanism for control flow. The routers are equipped with minimal input buffers and can optionally include output buffers, allowing a trade-off between reduced latency and improved timing closure for long routing channels [13]. Additionally, the internal switch of the router is optimized to disable loopbacks and exclude impossible connections under XY-Routing.

The router supports wormhole routing, which can be enabled on a flit basis. For instance, *W* bursts require wormhole routing to prevent interleaving with different streams of flits. The routing decision is handled by the *Routing* module, which was designed in a way that makes it easily extendable to a wide variety of routing algorithms. Currently, the router supports multiple static routing algorithms 1) *Source-based* routing, where the route through the network is computed at the source and encoded in the header of the flit 2) *Dimension-ordered-routing* which is applicable in 2D meshes 3) *Table-based* routing, where the output port for each *dstID* is stored in a routing table.

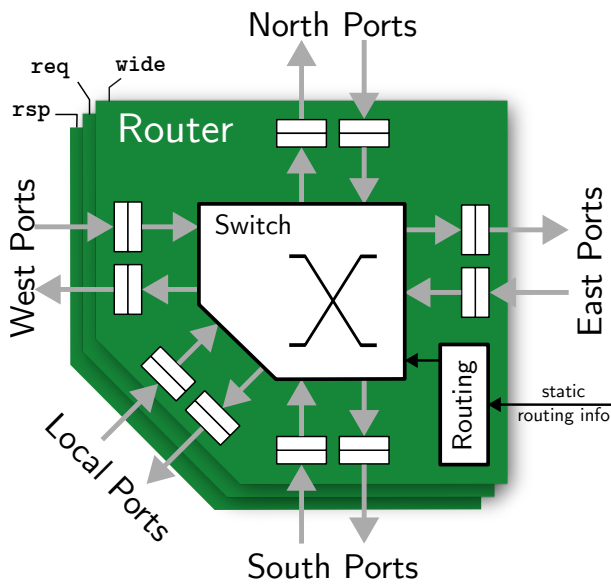


Fig. 4: Router microarchitecture of a 5×5 configuration with three links. Routing information such as local coordinates and routing tables are passed from externally.

IV. SYSTEM INTEGRATION

To properly assess its performance, a NoC should be integrated into a full SoC architecture and analyzed in context. We address this requirement in the following subsections.

A. Compute Tile

We integrate the AXI4-NI and router into a Snitch cluster [45], creating a compute tile, as illustrated in Figure 5. The router is configured for XY-Routing with 5×5 ports: one local port for the cluster and one port for each cardinal direction. The compute cluster comprises eight RISC-V cores with integrated Floating Point Units (FPUs) and a ninth RISC-V core dedicated to controlling the DMA. The Scratchpad Memory (SPM) and instruction cache, shared among all cores, are sized at 128 kB and 8 kB, respectively. The internal interconnect within the cluster includes a 512-bit wide AXI4 bus used by the DMA and L1 instruction cache to fetch large data blocks. Additionally, all RISC-V cores connect to a narrow 64-bit AXI4 bus for single-word remote accesses. Both the narrow and wide AXI4 buses are equipped with initiator and target ports, allowing the cluster's internal SPM to be accessed remotely by other clusters. The AXI4-NI is connected to both the narrow and wide AXI4 buses according to the mapping outlined in Table I.

1) *Ordering & Multi-Channel DMA*: We enable out-of-order transactions in the cluster in multiple ways. For both the narrow and the wide AXI4 interface, we configure the NI with the newly proposed *RoB-less* version instead of our previous work [22] for more cost-effective and performant end-to-end ordering. We prevent stalls that might occur from the ordering guarantee the following way: The narrow ports of each core in the Snitch cluster have unique IDs, which enables out-of-order responses from different cores by design. Only simultaneous accesses of the same core to different

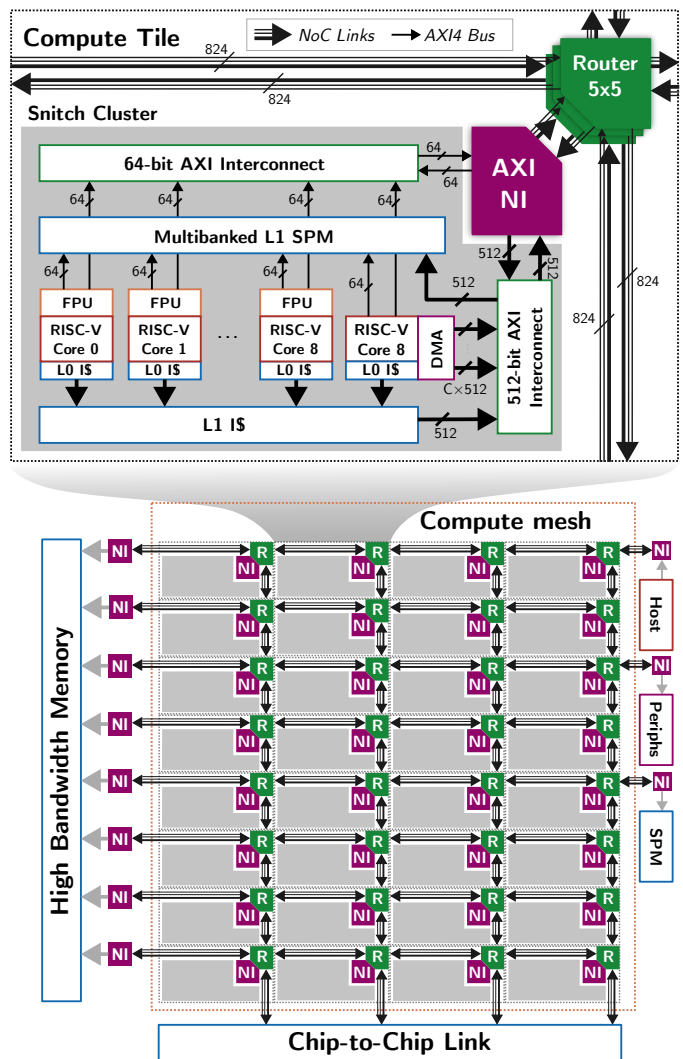


Fig. 5: *Top*: Compute tile consisting of a Snitch cluster with nine RISC-V compute cores, one of which is tightly-coupled to a DMA engine capable of handling C streams in parallel. An AXI4-NI attached to the wide 512-bit and narrow 64-bit AXI4 bus, and separate 5×5 router for each physical link in the narrow-wide network. *Bottom*: Compute mesh of 8×4 compute tiles. The compute mesh connects to the High Bandwidth Memory (HBM) on the left, to Chip-to-Chip (C2C)-link for off-chip communication on the bottom.

destinations might exhibit stalls. However, the compute cores mainly operate on the cluster-internal L1 SPM, and narrow traffic out of the cluster is rare and limited to synchronization between clusters, which should not be affected by stalls.

The wide AXI4 interface is the more critical component, which previously required a large RoB buffer [22] to ensure high performance. In this work, however, we extended the compute cluster with a multi-channel DMA [46] that allowed us to get rid of the RoB inside the NI and offload the ordering of different streams to the DMA itself. The DMA can be programmed through a single *frontend* that controls multiple *backends* of the DMA, each capable of handling a separate stream. The DMA has one wide 512-bit AXI4 port for each

backend, which is connected to the wide AXI4 Xbar, meaning each stream coming from a *backend* and entering the NI has a unique TxnID and does not imply any ordering with other streams.

B. Compute Mesh

The system can be scaled up by replicating the compute tile and arranging it as a homogeneous compute mesh of tiles, as shown in Figure 5. The top-level connects the NoC links of two neighboring tiles or ties them off if the tile is located at a boundary without any I/O components. Additional I/O components can be connected to the NoC with an additional NI that converts the NoC protocol back to AXI4 if required. For instance, the HBM controller is attached to the left side of the compute mesh. We match the bandwidth to the HBM by dimensioning the number of rows equal to the number of HBM channels. For multi-chiplet scaling, a C2C can be attached at the bottom of the compute mesh. Lastly, additional components such as a host processor, peripherals, and SPM are attached to the right side of the compute mesh.

V. PHYSICAL IMPLEMENTATION

We performed the physical implementation of a compute mesh with 8×4 compute tiles. We used a hierarchical design flow with SYNOPSIS FUSION COMPILER 2022.03 to synthesize, place, and route the compute mesh and tile in GLOBALFOUNDRIES' 12 nm FinFet technology.

A. Compute Tile

Most of the physical design effort was spent on the compute tile, which is replicated on the top-level to form a compute mesh. The floorplan of the tile was chosen to have an aspect ratio of 2:1 to maximize the horizontal bandwidth per coastline on the left side facing the HBM. As observed in [47], the most challenging component of the Snitch cluster is the fully-connected crossbar to the multi-banked L1 SPM since it is routing-bound. In order to utilize the full routing resources available inside a tile, we aimed to separate the routing-intensive SPM crossbar and the NoC links. First, We placed the memory macros of the SPM in a U-shape to the right of the floorplan to force the crossbar to the right side as well. Second, we placed the ports of the NoC links on the left, respectively, on the top side of the edge to pull the router away from the routing-bound crossbar. The result is seen in the annotated floorplan of the tile in Figure 6. The ports of the NoC were deliberately placed on the upper layers of the metal stack so that the global wires of the NoC links could easily be routed over the memory macros, which only occupy the bottom layers of the metal stack.

The input and output of the tile were constrained with 75 % of the clock period to reflect the fact that the signal from the neighboring tile has had to travel a large distance already. In order to ease the timing of the NoC links that need to bridge a distance >1 mm, we additionally configured the routers with output buffers. Further, we flattened the three routers directly into the compute tile instead of creating a macro. This has

multiple benefits: 1) The router can absorb the under-utilized routing resources from the surrounding logic [12] 2) The tool can spread out the input and output buffers over a larger area than a router macro, allowing it to meet the input and output timing more easily.

B. Compute Mesh

The physical design of the compute mesh mainly consisted of determining the aspect ratio of the floorplan and the placement of the *Compute Tiles* in a mesh structure. The height of the *Compute Mesh* was chosen to match the height of the HBM controller used in [48]. Further, the compute tiles were placed with a small gap between the top-level NoC connections. This gap is also used for routing the clock tree, which prevents a direct abutment of the tiles.

The entire *Compute Mesh* is one synchronous clock domain, and the timing closure was done in two steps. First, all *reg2reg* paths inside a *Compute Tile* were closed, and second, all paths on the top-level. The *in2reg* and *reg2out* paths on the *Compute Tile* level are not relevant for timing closure as long as the timing on all *tile2tile* paths can be met at the top-level. The maximum frequency is then determined by the Worst Negative Slack (WNS) of *Compute Tile* and *Compute Mesh*.

VI. RESULTS

We first evaluate the performance of the NoC in terms of latency and throughput and then discuss physical design results such as area, timing, and energy efficiency of the design. *FlooNoC* is implemented as SystemVerilog RTL, and performance was simulated with QUESTASIM 2023.4. Performance numbers were extracted from cycle-accurate traces of accesses issued by the cores and DMAs. Further, we used *DRAMSys* [49] with a configuration of eight Micron MT54A16G808A00AC-36 HBM2E channels to accurately model the latency and throughput of HBM accesses. The HBM2E model we used has a peak bandwidth of 57.6 GB/s per channel.

The area and timing numbers were extracted from the netlist of the placed and routed design in GLOBALFOUNDRIES' 12 nm FinFet technology with Static Timing Analysis (STA) of SYNOPSIS FUSION COMPILER 2022.03. Further, the same netlist was used to perform post-layout power simulations using SYNOPSIS PRIMETIME 2022.3 in typical conditions (TT, 0.8 V, 25 °C).

A. Bandwidth

Our NoC solution aims to provide a sustained high bandwidth data flow required by many applications today [5]. The cluster-internal DMA can handle large bursts of data while providing tolerance to latency due to the ability to issue multiple outstanding transactions at once. The 512-bit wide links in the NoC used by the DMAs achieve a peak bandwidth of 645 Gbps (1.29 Tbps duplex), operating at a frequency of 1.26 GHz. This allows for considerable bandwidth across the network, specifically tailored to handle the demands of high-volume data traffic directed toward memory controllers and

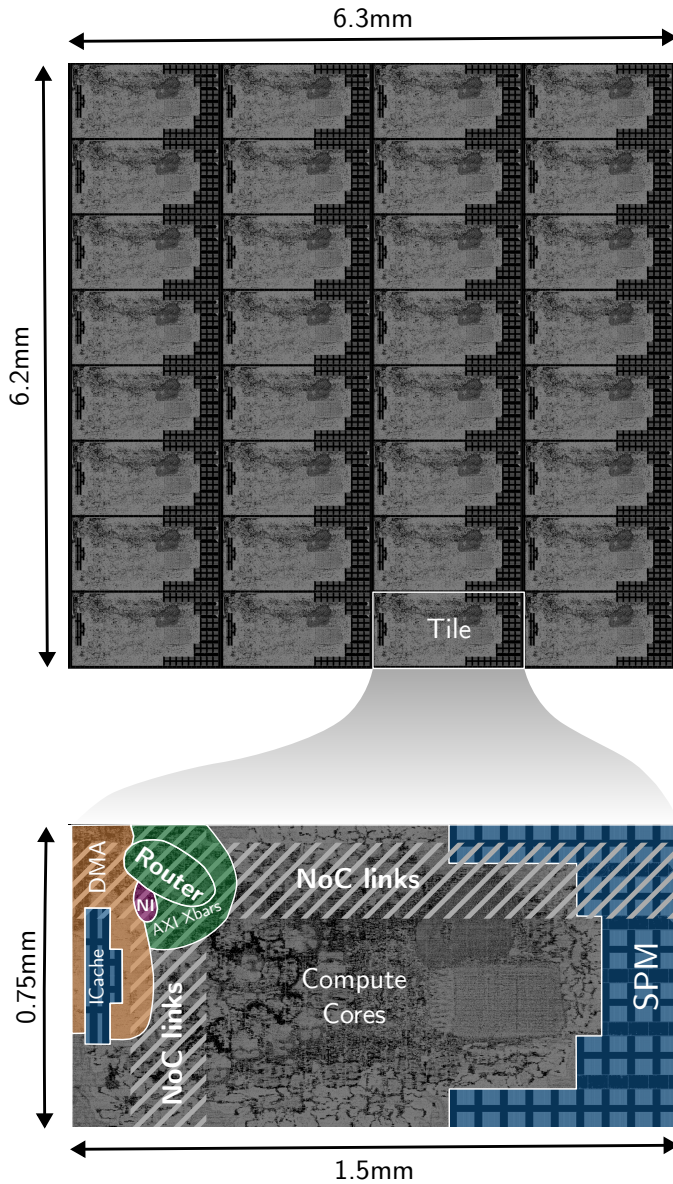


Fig. 6: *Top*: Placed and routed design of a *Compute Mesh* with 8×4 compute tiles. *Bottom*: Macro of a single compute tile, with annotated NoC components and NoC links.

I/O interfaces such as HBM controllers and C2C links. In the practical application within an 8×4 compute mesh, the NoC demonstrates an effective delivery of massive bandwidth at the boundary.

We also evaluate the bandwidth utilization achieved at the boundary when accessing HBM channels. We simulate the maximum bandwidth achieved where each tile accesses the HBM channel of its row in the mesh. Additionally, we simulate two different conditions: *zero-load*, where each tile is the only accessor of the HBM channel, and *full-load*, where all tiles in a row simultaneously access an HBM channel, representing a maximum contention scenario on each HBM channel. The results are shown in Figure 11a. Under the zero-load condition, the bandwidth utilization of an HBM2E channel (57.6 GB/s) is almost maximized, with most channels achieving near-optimal

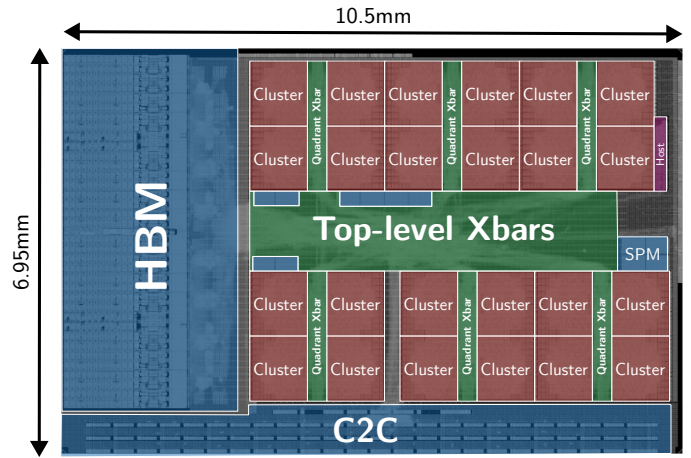


Fig. 7: Annotated die shot of *Occamy* with interconnect components depicted in green. The die shot also includes I/O components like HBM and C2C.

utilization levels of 97%. The observed decrease to 91% in one tile is due to increased contention with instruction fetches on the first HBM channel where the test binary is stored. These instruction fetches are counted towards the bandwidth utilization. In the full-load condition, each tile achieves up to 28% HBM bandwidth utilization and a full combined HBM bandwidth utilization in each row of the mesh. It is also noteworthy that the bandwidth distribution amongst the column of the tiles is fair, even if requests from the right tiles face more contention than tiles closer to the HBM channels, which has been reported to be a problem when using standard Round-Robin (RR) arbiters in the routers [50].

B. Latency

Apart from latency-tolerant burst-based traffic, we also measured the latency experienced by cores accessing the L1 SPM of another tile over the narrow NoC links. For instance, this type of traffic occurs during the synchronization of multiple clusters, which is much more latency-sensitive. A breakdown of the Tile-to-Tile access latency is shown in Figure 8.

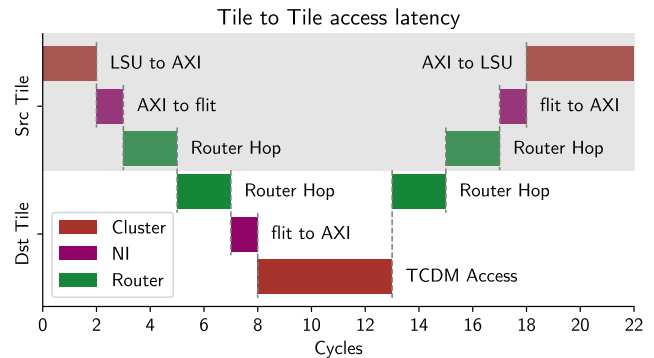


Fig. 8: Latency breakdown of a Tile to Tile access of a narrow transfer.

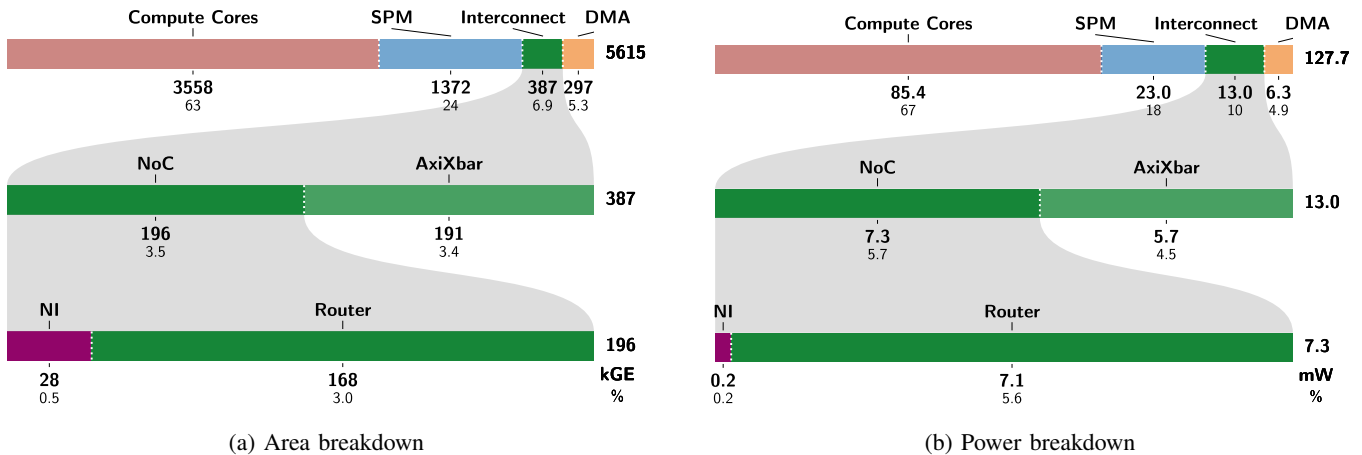


Fig. 9: post-layout area and power breakdowns of a single tile (a) Area breakdown of a single tile with integrated NoC components (b) Power breakdown of a tile during a 4 kB DMA transfer from tile to neighboring tile. All cores expect the DMA core to remain idle during the transfer.

Accessing a neighboring tile during *zero-load* results in a latency of 22 cycles, which includes the entire roundtrip of sending a read request and receiving the read data. Only eight of the total cycles are contributed from the NoC routers, where each hop has a cost of a two-cycle latency. Additionally, the NIs add three cycles of latency for translating an AXI4 request or response to a flit and vice-versa. The remaining latency comes from the cluster-internal interconnect as well as memory access latency. Each additional hop to access a non-neighboring tile costs four cycles. In the worst case, communication between two tiles can cost up to 58 cycles in an 8×4 mesh. The latency significantly increases when *full-load* is considered and can reach up to 321 cycle latency in the worst case when every core (a total of 279 cores) is accessing the same tile through the NoC. Note that this very unlikely scenario can be easily avoided in software. For instance, synchronization of all cores can be done hierarchically with intra-cluster followed by inter-cluster synchronization, which decreases the number of simultaneous accesses by $9 \times$.

C. Area & Timing

The area impact of the NoC components is small, as shown in the area breakdown in Figure 9a. The largest contributors to the total area of the tile are the compute cores, with the FPU, followed by the L1 SPM. The entire interconnect, which includes the NoC and the cluster-internal wide 512-bit AXI4 Xbar only occupies 6.9% of the area, which is almost evenly split between NoC and Xbar. The NoC complexity is largely dominated by the router, where 53% of the area is taken up by the Standard Cell Memory (SCM) input and output buffers while the rest is needed for the router switch.

The NI without a RoB is almost negligible in complexity with a compute tile, taking up only 25 kGE. This is possible thanks to the end-to-end optimization of AXI4 ordering in the DMA of the cluster. However, enabling multi-channel DMA comes at a cost, which is shown in Figure 10. The DMA complexity increases significantly for a 4-channel configuration, as it needs to handle multiple streams in parallel. Furthermore,

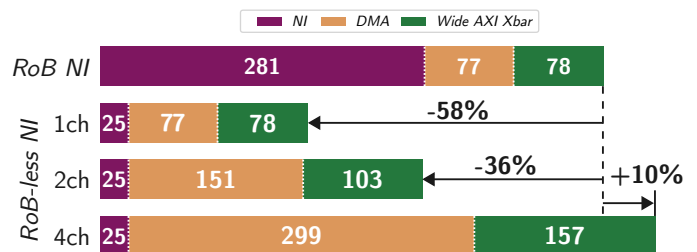


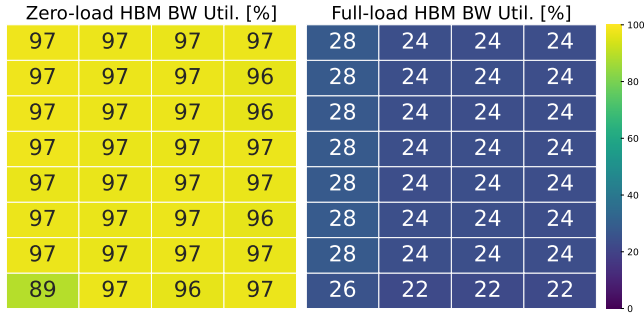
Fig. 10: Area breakdown in kGE of components in a tile affected by end-to-end ordering. Comparison between *RoB* and *RoB-less* configurations with 1-4 DMA channels are shown. The RoB has a size of 8 kB implemented as SRAMs.

each channel has its own AXI4 port to the cluster internal wide AXI4 Xbar, which causes another 50% increase in the size of the Xbar. Consequently, the area reduction in the NI is compensated in the DMA and Xbar, but with the benefit of having multiple parallel streams that do not interfere with each other and without performance degradation resulting from limited RoB capacity.

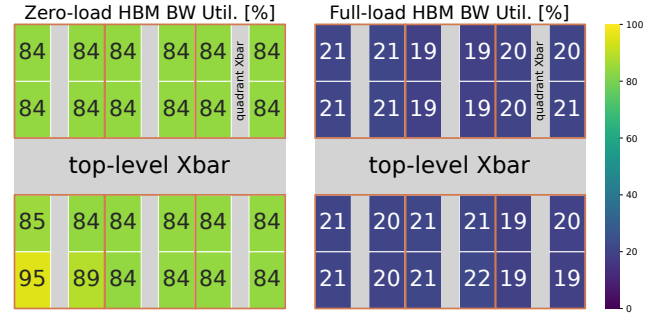
The critical path of the compute mesh is inside the Snitch cores of the compute cluster and is not affected by the NoC. The timing closes at 1.26 GHz in typical conditions (TT, 0.8 V, 25 °C), which corresponds to a delay of 67 FO4.

D. Energy & Power

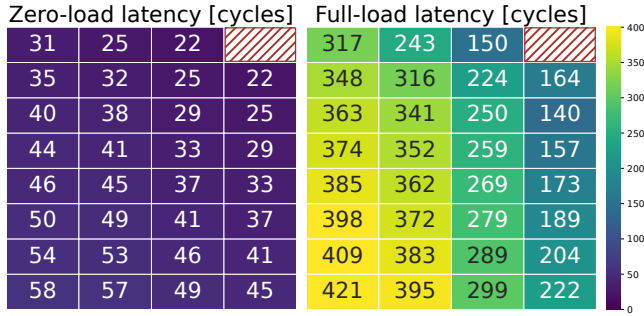
In our analysis, we simulated the power consumption involved in transferring 4 kB of data from one tile to a neighboring tile over the NoC, as detailed in Figure 9b. Although all eight compute cores remained idle during this transfer, they were the primary contributors to power consumption. This substantial usage is primarily due to the clock tree, which accounts for nearly 50% of the idle power usage, and leakage power, which constitutes another 10%. As a result, only about 15% of the total power of 127.7 mW is consumed by the components actively involved in the transfer (DMA, wide AXI4 Xbar & NoC). Consequently, the NoC



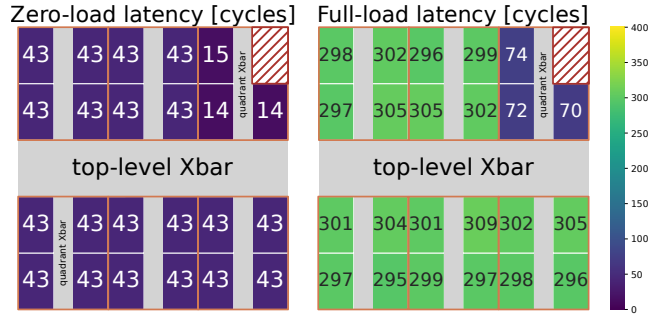
(a) Wide link utilization relative to the maximum HBM bandwidth of a channel in *FlooNoC* when each tile accesses one HBM channel (`tile_coord_y`).



(b) Utilization of the wide AXI4-bus relative to the maximum HBM bandwidth of a channel in *Occamy* when each cluster accesses one HBM channel (`cluster_id % #HBM_CHs`).



(c) Latency narrow reads to top right tile in *FlooNoC*



(d) Latency of narrow reads to top right cluster in *Occamy*

Fig. 11: Latency of narrow accesses and bandwidth utilization of the wide links in the 8×4 compute mesh and 6×4 *Occamy* organized by their physical location. During *zero-load* only one core or DMA issues requests and *full-load* all cores or DMAs issue request simultaneously. In the bandwidth simulations, each DMA issues 32TXNS of size 4KB.

is not the limiting factor in terms of power consumption on a system level. Furthermore, the routers only consume 596pJ during the transfer, resulting in an energy efficiency of 0.15 pJ/B/hop.

VII. SYSTEM-LEVEL COMPARISON

We also performed a system-level comparison with *Occamy*, which features the same compute clusters, but connects them with a hierarchical AXI4 interconnect instead of a mesh as is shown in the annotated die shot in Figure 7. On the lowest level of the hierarchy, *Occamy* groups together four clusters with an AXI4 Xbar for both the 64-bit narrow and the 512-bit wide interconnect to form a group. Further, six of those *groups* are connected with a top-level Xbar, that also connects the system with the HBM and C2C-link. We measured the performance of the *Occamy* system with the same setup, i.e., extracting the performance from cycle-accurate traces from RTL simulations and HBM modeling with *DRAMSys*. The area and timing numbers were generated from the area reports respectively STA from the database of the final design that was taped out.

A. Bandwidth

First, we compare the bandwidth of *Occamy* against *FlooNoC*-based systems. On a basic level, both designs rely on the wide and duplex 512-bit AXI4 bus for high-bandwidth traffic. However, the wide link in *FlooNoC* is shared amongst read

and write data in one direction, as explained in Section III-B, as opposed to a standard AXI4 bus, which defines separate R and W channels in each direction. In theory, the link sharing in *FlooNoC* would halve the bandwidth for concurrent read and write access from and to a tile. However, the L1 SPM has a bandwidth of only 512 bit/cycle, limiting the full utilization of R and W channels. Furthermore, the bandwidth achieved on a wide link (645 Gbps) is slightly higher than in *Occamy* (584 Gbps) due to the slightly higher maximum frequency.

We also compared the bandwidth utilization of the HBM channels that can be achieved in both systems, which is shown in Figure 11a and Figure 11b. In both the *zero-load* and *full-load* scenarios, *FlooNoC* achieves higher utilization. The reasons for the difference in bandwidth utilization are manifold. First, the top-level Xbar in *Occamy* had to be split up into a hierarchy of Xbars to make it even possible to implement physically, which increases the depth of the memory hierarchy and, consequently, the number of hops and latency. Second, the physical distances between Xbars in a hierarchical interconnect are much larger compared to a mesh that only connects neighboring tiles. Multiple spill registers must be inserted to bridge this distance, which again increases latency. Even though AXI4 supports multiple outstanding transactions to tolerate latency, the *zero-load* results show that increased latency can still impact the bandwidth. In *FlooNoC*, the latency to the nearest HBM channel is much lower, resulting in higher bandwidth overall.

The difference in HBM bandwidth utilization in the *full-load* is even more significant. Even though *FlooNoC* has more clusters than *Occamy*, a cluster in *FlooNoC* gets a larger share of the HBM bandwidth. The most obvious reason is that *FlooNoC* has one link to each HBM channel, while *Occamy* only has six (one from each cluster). Moreover, the AXI4 Xbars in *Occamy* does not support as many outstanding transactions as would be needed in the *full-load* case. In a hierarchical interconnect, AXI4 Xbars need to be configured to support progressively more outstanding transactions with each additional level, which becomes too expensive at some point. These issues limit the *full-load* HBM bandwidth utilization in *Occamy* to around 60% compared to near maximum utilization in *FlooNoC*.

B. Latency

Regarding latency, the hierarchical interconnect of *Occamy* has its merits in some cases. As is shown in Figure 11c and Figure 11d, the cluster-to-cluster access latency is slightly lower in *Occamy* when the access is happening inside a *group*, since it only consists of a single hop of an Xbar and also omits the latency induced by the NIs. On the other hand, access to a cluster in another *group* is much more costly, with 43 cycles of latency. The group-to-group latency in *Occamy* also does not depend on the distance, respectively, the location of the other *group*, which is more relevant in a mesh-based system where the latency depends on the number of hops throughout the network. This is visible in both the *zero-load* and *full-load* scenarios. While *FlooNoC* has a larger maximum latency in both scenarios, it represents the worst-case latency and can more easily be mitigated with physical awareness of the data. For instance, placing a synchronization barrier in the middle of the mesh will have an immediate positive effect on latency, while the latency in *Occamy* will remain constant and independent of the choice of cluster or *group*.

C. Area & Timing

FlooNoC demonstrates a notable improvement in area efficiency over *Occamy*, as detailed in Table II. The die shot in Figure 7 clearly shows that the top-level Xbar in *Occamy* occupies almost 40% of the compute domain². In contrast, an 8×3 compute mesh using *FlooNoC* achieves an 85% reduction in top-level area and 30% overall. Although integrating NoC components increases the complexity of a tile slightly by 8%, this is more than offset by the significant area savings at the top level. Moreover, an 8×4 compute mesh fits within the same floorplan as the compute domain in *Occamy*, which only features 24 clusters.

The integration of *FlooNoC* into the system does not adversely affect the overall timing in typical conditions, as the critical path in both systems resides in the compute cluster. However, *FlooNoC* achieves a slightly higher frequency of 1.26 GHz compared to 1.14 GHz in *Occamy*, which can be attributed to the slightly larger floorplan of the compute tile

²The compute domain only includes the cluster and AXI4 interconnects without HBM Ctrl./PHY and C2C-link

TABLE II: Comparison with AXI4-Xbar based *Occamy* and compute mesh based on *FlooNoC*

Metric	Occamy ^a [48]	FlooNoC	
		8×3 Mesh	8×4 Mesh
#Clusters	24	24 (+0%)	32 (+33%)
Peak GFLOPS _{DP} ^b	438	484 (+10%)	645 (+47%)
Peak BW to HBM [Tbps]	7.0	8.2 (+17%)	8.2 (+17%)
SS freq. [GHz]	0.88	0.90 (+2%)	0.85 (-3%)
TT freq. [GHz]	1.14	1.26 (+11%)	1.26 (+11%)
Die Area [mm ²]	42.1	29.5 (-30%)	39.3 (-7%)
Tile/Cluster Area [mm ²]	25.1	27.0 (+8%)	36.0 (+43%)
Top-level Area [mm ²]	16.7	2.5 (-85%)	3.3 (-80%)
Compute density [GFLOPS _{DP} /mm ²]	10.4	16.4 (+58%)	16.4 (+58%)

^aconsidering only the compute domain of a single chiplet w/o HBM, C2C
^b TT frequency

compared to the cluster floorplan in *Occamy*. This results in a performance improvement of 10% in terms of GFLOPS_{DP} for a 24-cluster system. Furthermore, *FlooNoC* achieves a significantly higher compute density of 16.4 GFLOPS_{DP}/mm², 58% higher than *Occamy*. This allows the integration of an additional eight clusters, which still fit into the same floorplan as *Occamy*.

VIII. COMPARISON WITH SOA

We also compare our physical implementation of the 8×4 compute mesh with the SoA in Table III. Most of the previous work uses 2D-mesh topology, mainly due to the advantages during physical implementation. *Piton* [51], for instance, employs a 5×5 mesh of tiles of cores with routers for three physical channels. While their NoC is very inexpensive in terms of area utilization, the narrow 64-bit links cannot match the bandwidth provided by the wide links of *FlooNoC*. They also report silicon measurements for energy efficiency in a 32 nm technology, which are $3 \times$ higher than our power simulations. More recent work has optimized the *Piton* NoC for HPC [37], with wider links up to 512 bit, but is missing a physical implementation. The *Celerity* chip [52] achieves a very high aggregate NoC bandwidth thanks to its more fine-grained tiling approach. However, they end up with a much lower tile-to-tile bandwidth that is ultimately limited by the very narrow link size of 32 bit. Another, more exploratory, work on physical implementation [44] used larger link sizes up to 256 bit to achieve a higher tile-to-tile bandwidth up to 256 Gbps. However, the tile in which they integrated the NoC is very small, resulting in a very high area overhead of more than a third of the tile area. Lastly, the *ESP*-NoC uses a slightly different approach, using six physical channels that achieve a respectable tile-to-tile bandwidth of 310 Gbps. However, the NoC contributes 23% to the total SoC's power consumption of 501 mW, and the energy efficiency cannot match *FlooNoC*'s.

IX. CONCLUSION

In this paper, we presented an open-source NoC design with full AXI4 support, tailored to handle the significant bandwidth demands of today's data-intensive applications. Our approach,

TABLE III: Comparison of State-of-the-Art systems with NoCs

Work	Piton [51]	Celerity [52]	Ou et al. [44]	ESP [30]	Prev. work [22]	This work
Technology	32nm SOI	16nm FinFET	14nm	12nm FinFET	12nm FinFET	12nm FinFET
Voltage	1.0V	0.98 V	-	0.8 V	0.8 V	0.8 V
Frequency	0.5 GHz	1.4 GHz	1 GHz	0.8 GHz	1.23 GHz	1.26 GHz
Measurement setup	silicon	silicon	post-layout	silicon	post-layout	post-layout
Num Tiles	25 (5 × 5 mesh)	496 (8 × 62 mesh)	256 (16 × 16 mesh)	34 (6 × 6 mesh)	1 ^e	32 (8 × 4 mesh)
Die Area	36 mm ²	12.3 mm ²	n.A. ^e	64 mm ²	1.1 mm ²	39 mm ²
NoC Area	0.84 mm ²	0.93 mm ²	n.A. ^e	n.A.	0.11 mm ²	1.37 mm ²
NoC/Die Area Ratio	2.9 %	7.77 %	18.2 % ^c /35.3 % ^d	n.A.	10 %	3.5 %
Tile-to-Tile NoC BW ^a	96 Gbps	45 Gbps	256 Gbps	310 Gbps	787 Gbps	806 Gbps
Aggregate NoC BW	4 Tbps	361 Tbps	n.A. ^e	74 Tbps	n.A. ^e	103 Tbps
Energy-efficiency	0.45 pJ/B/hop	n.A.	n.A.	2.0 pJ/B/hop	0.19 pJ/B/hop	0.15 pJ/B/hop
NoC Power contrib.	n.A.	n.A.	n.A.	23 %	7 %	5.7 %
Virt. Channels	×	×	×	×	×	×
Multiple Phys. Channels	✓(3)	×	×	✓(6)	✓(3)	✓(3)
Link Data Width	64	32	256	64	2×64 + 512	2×64 + 512

^asimplex, counting only data-bits ^c4 dummy tile of size 0.14 mm² ^dc1 dummy tile of size 0.034 mm² ^e only single tile

which utilizes wide links, leverages advancements in modern technologies that make it physically feasible to accommodate an increased number of wires without the need for frequency multiplication.

Implemented in a 12 nm VLSI technology, an 8×4 compute mesh with 288 RISC-V cores has a low area overhead of just 3.5% per compute tile. It delivers extremely high bandwidth, achieving up to 645 Gbps per link and a total aggregate bandwidth of 103 Tbps. The NoC's unique end-to-end ordering system, powered by a multi-stream capable DMA, simplifies the NI and eliminates inter-stream dependencies, enhancing scalability and efficiency. These improvements led to a 30% reduction in area and a 47% increase in GFLOPS_{DP} within the same floorplan compared to a traditional AXI4-based SoC. Our design significantly outperforms current state-of-the-art NoCs, offering up to three times the energy efficiency and more than double the tile-to-tile bandwidth.

ACKNOWLEDGMENT

The authors thank Tobias Senti for his valuable contributions to this work. We utilized ChatGPT by OpenAI, for enhancing text readability and grammar across this manuscript. The use of AI was limited to text improvement and did not contribute to original content or research findings.

REFERENCES

- [1] R. Kaplan, "Intel gaudi 3 ai accelerator: Architected for gen ai training and inference," in *2024 IEEE Hot Chips 36 Symposium (HCS)*, 2024.
- [2] M. Maddury and P. Kansal, "Next gen mtia - meta's recommendation inference accelerator," in *2024 IEEE Hot Chips 36 Symposium (HCS)*, 2024.
- [3] S. Xu and C. Ramakrishnan, "Inside maia 100," in *2024 IEEE Hot Chips 36 Symposium (HCS)*, 2024.
- [4] A. Gholami, Z. Yao et al., "Ai and memory wall," *IEEE Micro*, vol. 44, no. 3, pp. 33–39, 2024.
- [5] S. Kim, C. Hooper et al., "Squeezellm: Dense-and-sparse quantization," 2024. [Online]. Available: <https://arxiv.org/abs/2306.07629>
- [6] T. Krishna, L.-S. Peh et al., "Towards the ideal on-chip fabric for 1-to-many and many-to-1 communication," in *Proceedings of the 44th Annual IEEE/ACM International Symposium on Microarchitecture*, 2011, pp. 71–82.
- [7] J. Lee, C. Nicopoulos et al., "Do we need wide flits in networks-on-chip?" in *2013 IEEE Computer Society Annual Symposium on VLSI (ISVLSI)*, 2013, pp. 2–7.
- [8] International Roadmap for Devices and Systems, "Ird's roadmap report," IEEE, Tech. Rep., 2017-2022, accessed: 2024-05-02. [Online]. Available: <https://irds.ieee.org/editions>
- [9] R. Brain, "Interconnect scaling: Challenges and opportunities," in *2016 IEEE International Electron Devices Meeting (IEDM)*, 2016, pp. 9.3.1–9.3.4.
- [10] N. E. Jerger, T. Krishna, and L.-S. Peh, *On-chip networks*. Springer Nature, 2022.
- [11] W. Dally, "Reflections on 21 years of NoCs," 2022, 16th IEEE/ACM International Symposium on Networks-on-Chip. [Online]. Available: <https://nocs2022.github.io/program.html#KeynoteII>
- [12] D. Petrisko, C. Zhao et al., "Noc symbiosis (special session paper)," in *2020 14th IEEE/ACM International Symposium on Networks-on-Chip (NOCS)*, 2020, pp. 1–8.
- [13] G. Dimitrakopoulos, A. Psarras, and I. Seitanidis, *Microarchitecture of Network-on-chip Routers*. Springer, 2015, vol. 1025.
- [14] A. Kurth, W. Rönninger et al., "An open-source platform for high-performance non-coherent on-chip communication," *IEEE Transactions on Computers*, vol. 71, no. 8, pp. 1794–1809, 2022.
- [15] L. Benini and G. De Micheli, "Networks on chips: a new soc paradigm," *Computer*, vol. 35, no. 1, pp. 70–78, 2002.
- [16] T. Jia, P. Mantovani et al., "A 12nm Agile-Designed SoC for Swarm-Based Perception with Heterogeneous IP Blocks, a Reconfigurable Memory Hierarchy, and an 800MHz Multi-Plane NoC," in *ESSCIRC 2022- IEEE 48th European Solid State Circuits Conference (ESSCIRC)*, 2022, pp. 269–272.
- [17] S. Davidson, S. Xie et al., "The Celerity Open-Source 511-Core RISC-V Tiered Accelerator Fabric: Fast Architectures and Design Methodologies for Fast Chips," *IEEE Micro*, vol. 38, no. 2, pp. 30–41, 2018.
- [18] J. Balkind, M. McKeown et al., "Openpiton: An open source manycore research framework," *ACM SIGPLAN Notices*, vol. 51, no. 4, pp. 217–232, 2016.
- [19] ARM. (2019) CoreLink NIC for SoC Connectivity. [Online]. Available: <https://www.arm.com/products/silicon-ip-system/corelink-interconnect/nic>
- [20] J.-J. Lecler and G. Baillieu, "Application driven network-on-chip architecture exploration & refinement for a complex soc," *Design Automation for Embedded Systems*, vol. 15, no. 2, pp. 133–158, 2011.
- [21] SignatureIP. (2024) Non-Coherent NoC (NC-NoC). [Online]. Available: <https://www.signatureip.ai/NCNoc>
- [22] T. Fischer, M. Rogenmoser et al., "Floonoc: A multi-tb/s wide noc for heterogeneous axi4 traffic," *IEEE Design & Test*, vol. 40, no. 6, pp. 7–17, 2023.
- [23] M. Daneshalab, M. Ebrahimi et al., "Memory-efficient on-chip network with adaptive interfaces," *IEEE Transactions on Computer-Aided Design of Integrated Circuits and Systems*, vol. 31, no. 1, pp. 146–159, 2012.
- [24] W.-C. Kwon, S. Yoo et al., "A practical approach of memory access parallelization to exploit multiple off-chip ddr memories," in *Proceedings of the 45th annual Design Automation Conference*, 2008, pp. 447–452.

- [25] W. J. Dally and B. Towles, "Route packets, not wires: on-chip interconnection networks," in *Proceedings of the 38th annual design automation conference*, 2001, pp. 684–689.
- [26] ARM. (2013) AMBA AXI and ACE Protocol Specification Version E. [Online]. Available: <https://developer.arm.com/documentation/ih0022/e/>
- [27] V. Jain, M. Cavalcante *et al.*, "Patronoc: Parallel axi transport reducing overhead for networks-on-chip targeting multi-accelerator dnn platforms at the edge," in *2023 60th ACM/IEEE Design Automation Conference (DAC)*. IEEE, 2023, pp. 1–6.
- [28] B. Wang and Z. Lu, "Efficient support of axi4 transaction ordering requirements in many-core architecture," *IEEE Access*, vol. 8, pp. 182 663–182 678, 2020.
- [29] W.-C. Kwon, S. Yoo *et al.*, "In-network reorder buffer to improve overall noc performance while resolving the in-order requirement problem," in *2009 Design, Automation & Test in Europe Conference & Exhibition*, 2009, pp. 1058–1063.
- [30] M. C. Dos Santos, T. Jia *et al.*, "14.5 a 12nm linux-smp-capable risc-v soc with 14 accelerator types, distributed hardware power management and flexible noc-based data orchestration," in *2024 IEEE International Solid-State Circuits Conference (ISSCC)*, vol. 67, 2024, pp. 262–264.
- [31] A. S. Cassidy, J. V. Arthur *et al.*, "11.4 ibm northpole: An architecture for neural network inference with a 12nm chip," in *2024 IEEE International Solid-State Circuits Conference (ISSCC)*, vol. 67, 2024, pp. 214–215.
- [32] Y. J. Yoon, N. Concer *et al.*, "Virtual channels and multiple physical networks: Two alternatives to improve noc performance," *IEEE Transactions on Computer-Aided Design of Integrated Circuits and Systems*, vol. 32, no. 12, pp. 1906–1919, 2013.
- [33] F. Gilabert, M. E. Gómez *et al.*, "Improved utilization of noc channel bandwidth by switch replication for cost-effective multi-processor systems-on-chip," in *2010 Fourth ACM/IEEE International Symposium on Networks-on-Chip*, 2010, pp. 165–172.
- [34] D. C. Jung, S. Davidson *et al.*, "Ruche networks: Wire-maximal, no-fuss nocs : Special session paper," in *2020 14th IEEE/ACM International Symposium on Networks-on-Chip (NOCS)*, 2020, pp. 1–8.
- [35] W. Zhou, Y. Ouyang *et al.*, "Energy-efficient multiple network-on-chip architecture with bandwidth expansion," *IEEE Transactions on Very Large Scale Integration (VLSI) Systems*, vol. 31, no. 4, pp. 442–455, 2023.
- [36] T. C. Fischer, A. K. Nivarti *et al.*, "9.1 d1: A 7nm ml training processor with wave clock distribution," in *2023 IEEE International Solid-State Circuits Conference (ISSCC)*, 2023, pp. 8–10.
- [37] N. Leyva, A. Monemi *et al.*, "Openpiton4hpc: Optimizing openpiton towards high performance manycores," *IEEE Journal on Emerging and Selected Topics in Circuits and Systems*, pp. 1–1, 2024.
- [38] M. McKeown, Y. Fu *et al.*, "Piton: A manycore processor for multitenant clouds," *IEEE Micro*, vol. 37, no. 2, pp. 70–80, 2017.
- [39] S. Jain, H. Tsai *et al.*, "A heterogeneous and programmable compute-in-memory accelerator architecture for analog-ai using dense 2-d mesh," *IEEE Transactions on Very Large Scale Integration (VLSI) Systems*, vol. 31, no. 1, pp. 114–127, 2023.
- [40] R. Sambangi, A. S. Pandey *et al.*, "Application mapping onto manycore processor architectures using active search framework," *IEEE Transactions on Very Large Scale Integration (VLSI) Systems*, vol. 31, no. 6, pp. 789–801, 2023.
- [41] W. Zhao, G. Yang *et al.*, "Hipu: A hybrid intelligent processing unit with fine-grained isa for real-time deep neural network inference applications," *IEEE Transactions on Very Large Scale Integration (VLSI) Systems*, vol. 31, no. 12, pp. 1980–1993, 2023.
- [42] S. Lie, "Cerebras architecture deep dive: First look inside the hardware/software co-design for deep learning," *IEEE Micro*, vol. 43, no. 3, pp. 18–30, 2023.
- [43] R. Beachler and M. Snelgrove, "Untether ai : Boqueria," in *2022 IEEE Hot Chips 34 Symposium (HCS)*, 2022, pp. 1–19.
- [44] Y. Ou, S. Agwa, and C. Batten, "Implementing low-diameter on-chip networks for manycore processors using a tiled physical design methodology," in *2020 14th IEEE/ACM International Symposium on Networks-on-Chip (NOCS)*, 2020, pp. 1–8.
- [45] F. Zaruba, F. Schuiki *et al.*, "Snitch: A Tiny Pseudo Dual-Issue Processor for Area and Energy Efficient Execution of Floating-Point Intensive Workloads," *IEEE Transactions on Computers*, vol. 70, no. 11, pp. 1845–1860, 2021.
- [46] T. Benz, M. Rogenmoser *et al.*, "A high-performance, energy-efficient modular dma engine architecture," *IEEE Transactions on Computers*, vol. 73, no. 1, pp. 263–277, 2024.
- [47] G. Paulin, M. Cavalcante *et al.*, "Soft tiles: Capturing physical implementation flexibility for tightly-coupled parallel processing clusters," in *2022 IEEE Computer Society Annual Symposium on VLSI (ISVLSI)*. IEEE, 2022, pp. 44–49.
- [48] G. Paulin, P. Scheffler *et al.*, "Ocamy: A 432-core 28.1 dp-gflop/s/w 83% fpu utilization dual-chiplet, dual-hbm2e risc-v-based accelerator for stencil and sparse linear algebra computations with 8-to-64-bit floating-point support in 12nm finfet," *VLSI Symposium*, 2024.
- [49] M. Jung, C. Weis, and N. Wehn, "Dramsys: A flexible dram subsystem design space exploration framework," *IPSI Transactions on System and LSI Design Methodology*, vol. 8, pp. 63–74, 2015.
- [50] S. K. Mandal, S. Y. Narayana *et al.*, "Fast performance analysis for nocs with weighted round-robin arbitration and finite buffers," *IEEE Transactions on Very Large Scale Integration (VLSI) Systems*, vol. 31, no. 5, pp. 670–683, 2023.
- [51] M. McKeown, A. Lavrov *et al.*, "Power and energy characterization of an open source 25-core manycore processor," in *HPCA*, 2018, pp. 762–775.
- [52] A. Rovinski, C. Zhao *et al.*, "Evaluating celerity: A 16-nm 695 gigarisc-v instructions/s manycore processor with synthesizable pll," *IEEE Solid-State Circuits Letters*, vol. 2, no. 12, pp. 289–292, 2019.



Tim Fischer received his BSc and MSc in "Electrical Engineering and Information Technology" from the Swiss Federal Institute of Technology Zurich (ETHZ), Switzerland, in 2018 and 2021, respectively. He is currently pursuing a Ph.D. degree at ETH Zurich in the Digital Circuits and Systems group led by Prof. Luca Benini. His research interests include scalable and energy-efficient interconnects for both on-chip and off-chip communication.



Michael Rogenmoser received his BSc and MSc in "Electrical Engineering and Information Technology" from the Swiss Federal Institute of Technology Zurich (ETHZ), Switzerland, in 2020 and 2021, respectively. He is currently pursuing a Ph.D. degree in the Digital Circuits and Systems group of Prof. Benini. His research interests include fault-tolerant processing architectures and multicore heterogeneous SoCs for space.



Thomas Benz received the B.Sc. and M.Sc. degrees in electrical engineering and information technology from ETH Zurich, in 2018 and 2020, respectively. He is currently working toward the Ph.D. degree with the Digital Circuits and Systems group of Prof. Benini. His research interests include energy-efficient high-performance computer architectures and the design of ASICs.



Frank Gürkaynak received the BSc and MSc degrees in electrical engineering from the Istanbul Technical University, and the PhD degree in electrical engineering from ETH Zurich in 2006. He is currently working as a senior scientist with the Integrated Systems Laboratory, ETH Zurich. His research interests include digital low-power design and cryptographic hardware.



Luca Benini holds the chair of digital Circuits and systems at ETHZ and is Full Professor at the Università di Bologna. He received a Ph.D. from Stanford University. Dr. Benini's research interests are in energy-efficient parallel computing systems, smart sensing micro-systems and machine learning hardware. He is a Fellow of the IEEE, of the ACM and a member of the Academia Europaea.